Appl Phys B (2009) 97: 811–815
DOI 10.1007/s00340-009-3714-6

Applied Physics B
Lasers and Optics

Charge transport properties of undoped congruent lithium niobate crystals

M. Kösters · C. Becher · D. Haertle · B. Sturman · K. Buse

Received: 3 August 2009 / Published online: 12 September 2009

Abstract Time-resolved light-induced birefringence measurements based on a phase compensation technique are used to determine the charge transport properties of congruent, nominally-undoped lithium niobate crystals ($LiNbO_3$). Some of the crystals are conventionally oxidized. The steady-state space-charge field E_{pv}, the bulk photovoltaic coefficient β, and the photoconductivity σ_{ph} are determined in the intensity range (30–30 000) W/cm^2. The photovoltaic coefficient β increases by one order of magnitude over this intensity range, the space-charge field E_{pv} even by two orders of magnitude. We discuss the results in the context of the known one- and two-center charge transport models for $LiNbO_3$. The experimental findings presented here are of relevance for the long-standing problem of optical damage in such crystals, which inhibits their use in high-intensity applications like nonlinear optics.

PACS 77.84.Dy · 72.40.+w · 42.25.Lc · 78.20.-e

1 Introduction

Nominally-undoped lithium niobate crystals ($LiNbO_3$) become increasingly important for nonlinear optics because of their unique combination of physical properties: the crystals are transparent in the visible-to-infrared range, they provide excellent electro-optic and nonlinear-optical characteristics, and allow domain structuring for quasi-phase-matching [1–3].

So far, the main obstacle for the application of nominally-undoped $LiNbO_3$ in combination with high light intensities is the so-called "optical damage" [4, 5], the unwanted appearance of the photorefractive effect: the bulk photovoltaic effect causes a charge redistribution, space-charge fields build up and modulate the refractive index because of the linear electro-optic effect [6]. These light-induced refractive index changes lead to beam deterioration and, in particular, destroy the phase matching [5, 7]. Resolving this long-standing problem requires detailed knowledge of the charge transport properties of nominally-undoped $LiNbO_3$, in particular at high light intensities, both continuous wave (cw) and pulsed.

The photoelectric properties of $LiNbO_3$ crystals, which are moderately or strongly doped (10^{17}–10^{20} cm^{-3}), e.g. with iron, at low light intensities ($\lesssim$10 W/cm^2) are well-investigated [8, 9]: The bulk photovoltaic current density j_{pv} and the photoconductivity σ_{ph} are proportional to the light intensity I. In the absence of space-charge limitations, the steady-state value of the space-charge field is the bulk photovoltaic field $E_{pv} = j_{pv}/\sigma_{ph}$, which does not depend on I. The rise time is inversely proportional to the photoconductivity σ_{ph}. All these dependences, as well as the dependences of j_{pv}, σ_{ph}, and E_{pv} on conventional oxidization treatments, can be explained within the one-center model [5, 10, 11]. At sufficiently high intensities, E_{pv} is growing. This growth can be explained within the two-center model. A second more shallow center is supposed to be populated at higher intensities and to have a larger bulk photovoltaic coefficient than the deeper center, which is considered in the one-center model [8, 12, 13].

In contrast, the situation in nominally-undoped $LiNbO_3$ crystals is far from clear. The photorefractive effect in such

M. Kösters (✉) · C. Becher · D. Haertle · K. Buse
Institute of Physics, University of Bonn, Wegelerstr. 8, 53115 Bonn, Germany
e-mail: koesters@physik.uni-bonn.de

B. Sturman
Institute of Automation and Electrometry, Koptyug Ave. 1, 630090 Novosibirsk, Russia

crystals is attributed to a very low concentration of photorefractive impurity centers ($\leq$1 ppm), predominantly iron, which is inherent to the production process. The photorefractive sensitivity of such crystals is very low. Thus investigation of the photoelectric parameters, e.g. the photoconductivity, requires light intensities in the range of (10^1–10^5) W/cm^2. Experiments with cw light of such high intensities can be accomplished only by using focused light beams or wave-guiding structures; two-beam coupling schemes are not useful in this regime. Furthermore, the low concentration of photorefractive centers limits absorption measurements to very thick samples.

For these reasons, the photoelectric and the photorefractive properties of nominally-undoped $LiNbO_3$ crystals have remained almost uninvestigated, except for very few experiments [12, 14].

In this article, we present experimental data on the intensity dependences of the relevant quantities characterizing the photorefractive effect in nominally-undoped $LiNbO_3$ in the intensity range (30–30 000) W/cm^2. Measurements of light-induced birefringence changes, based on a phase compensation method [15, 16], with focused cw laser light are used to determine the steady-state space-charge field $E_{pv}(I)$, the photovoltaic coefficient $\beta(I)$, and the photoconductivity $\sigma_{ph}(I)$. Additionally, the impact of a conventional oxidization scheme [18, 19] onto the charge transport properties of nominally-undoped $LiNbO_3$ is investigated.

The results of our measurements are of relevance for gaining a better understanding of the origin of optical damage. In particular, they will help to optimize the experimental parameters of a method that we call "optical cleaning", which is promising for suppression of the photorefractive effect [20].

2 Experimental methods

An electric field E_z applied along the z-axis of a $LiNbO_3$ crystal leads to different electro-optic refractive index changes $\Delta n_{o,e}$ for ordinarily and extraordinarily polarized waves. The resulting change of the birefringence is given by $\delta n = \Delta n_e - \Delta n_o = (n_e^3 r_{33} - n_o^3 r_{13}) E_z/2$, where $n_{o,e}$ are the initial refractive indices for ordinary and extraordinary polarization, and r_{33} and r_{13} are the relevant electro-optic coefficients. It can be measured using a phase compensation technique [15, 16]. The method allows for the determination of birefringence changes as small as 10^{-5} for our crystal thicknesses. Thus finally E_z can be obtained. Both, the refractive indices and the electro-optic coefficients, are well known for $LiNbO_3$ [21, 22].

The experimental setup is shown in Fig. 1. A weak Gaussian laser beam at 633 nm with an $1/e^2$ radius at the beam waist of $w_{633} = 15$ µm and a peak intensity of

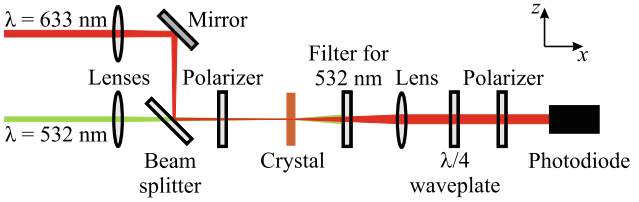

Fig. 1 Experimental realization of the phase compensation technique used for the time-resolved light-induced birefringence measurements

$I_0 = 0.1$ W/cm^2 is used to probe the birefringence changes. This beam is polarized at 45° with respect to the optical (z-) axis of the crystal.

Build-up of the electric space-charge field and thus of the birefringence changes is accomplished by illumination of the samples with a focused Gaussian beam at the wavelength 532 nm impinging onto the x-face of the crystal. This intense beam propagates co-axially to the weak probe beam. Two different $1/e^2$ radii at the beam waist are used: $w_{532} = 30$ µm and 80 µm. The peak intensity can be varied from $I_0 = (30$–$30\,000)$ W/cm^2.

An important feature of our setup is the use of focused light beams with a 2D Gaussian intensity distribution. For 1D light patterns, the recording kinetics of the refractive index changes follows a mono-exponential behavior $E_z = E_{pv}[1 - \exp(-t/t_d)]$, where the dielectric relaxation time t_d is inversely proportional to the photoconductivity σ_{ph} [5, 23]. This allows for an easy extraction of E_{sat} and $\sigma_{ph}(I)$ from the recording data. The situation for 2D light patterns is different [17]: The recording kinetics is not monoexponential, even for isotropic media. Extraction of the charge transport parameters in this case requires the determination of the initial slope $dE_z(t)/dt$ and the steady-state space-charge field E_{sat} at the beam center. In the absence of space-charge limitations, this E_{sat} is the photovoltaic field $E_{pv} = \beta I_0/\sigma_{ph}$. The photovoltaic coefficient β at the beam center can then be determined using the relation [17]

$$\left.\frac{dE_z(t)}{dt}\right|_{t=0} = \frac{\beta I_0}{\varepsilon_0(\varepsilon_\parallel + \sqrt{\varepsilon_\parallel \varepsilon_\perp})}, \tag{1}$$

where $\varepsilon_\perp = \varepsilon_{yy} = 85$ and $\varepsilon_\parallel = \varepsilon_{zz} = 28.7$ are the transverse and longitudinal dielectric constants [22].

The photoconductivity σ_{ph} at the beam center can be obtained using the relation

$$\sigma_{ph} = \frac{1}{E_{pv}} \left.\frac{dE_z(t)}{dt}\right|_{t=0} = \frac{\beta I}{E_{pv}}. \tag{2}$$

The above relations, referring to the initial and steady-state stages of the build-up process, remain valid also in the case of intensity dependent E_{pv}, β, and σ_{ph}.

The samples studied are cut out of a nominally-undoped, congruently-melting x-cut $LiNbO_3$ wafer from the *Crystal Technologies, Inc*. For investigation of the impact of a conventional oxidization, some of the crystals are subjected to an annealing treatment at 1 000°C in normal atmosphere for different times in the range (1–50) h. The thickness of these samples in x-direction is $d = 1$ mm.

In addition, two special crystals of the same boule are used to study a possible dependence of the results on the crystal thickness d: a wedge crystal with extensions in x-direction in the range (0.1–0.8) mm and a thin crystal with a thickness $d = 0.1$ mm.

3 Experimental results

In a first series of experiments, the differently oxidized 1-mm-thick samples are investigated. For these experiments, the radius of the recording beam is kept at $w_{532} = 30$ µm. Strong changes of the birefringence are detected. Thermooptic effects can be excluded in our case. Measurements with a thermo camera showed, that the light-induced temperature change in the crystals is much less than 0.2°C. Therefore we attribute the index changes to the photorefractive effect.

Figure 2 shows the build-up of the space-charge field under illumination with the recording beam at a peak intensity of 100 W/cm^2 for an as-grown sample. It is obvious that the kinetics does not follow a monoexponential behavior. Thus, the initial slope of the evolution of the electric space-charge field $dE_z(t)/dt$ (dashed rising line) and its saturation value E_{pv} (dashed horizontal line) are taken to determine the photoelectric parameters β and σ_{ph} according to (1) and (2). For the data shown in Fig. 2, this gives $E_{pv} = 6.8$ kV/cm, $\beta = 3 \times 10^{-12}$ A/W, and $\sigma_{ph} = 4 \times 10^{-14}$ Ω^{-1}cm^{-1}.

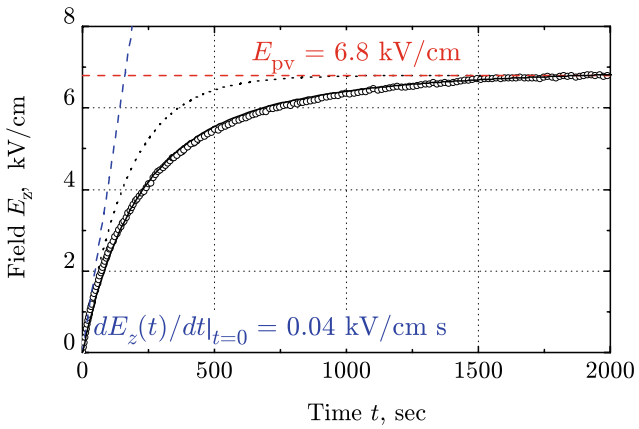

Fig. 2 Build-up of the electric space charge field $E_z(t)$ for a peak intensity of the recording beam of $I_0 = 100$ W/cm^2 (*open dots*). The *solid line* is a fit according to the non-exponential model [17], while the dotted line is a monoexponential fit. The *dashed lines* indicate the initial slope $dE_z(t)/dt$ and the steady-state space charge field E_{pv}

Evaluation of all the data sets for the differently oxidized crystals and different recording intensities I_0 leads to the intensity dependences shown in Fig. 3a–c for the photovoltaic field E_{pv}, the photovoltaic coefficient β, and the photoconductivity σ_{ph}. In order to get an estimate of the variance of the results, we repeat for each crystal and intensity the measurements three times at different crystal positions. The data points in Fig. 3 are the mean values of these measurements; the error bars indicate the variance.

According to Fig. 3a, the steady-state values of the field E_{pv} increase sublinearly (as $\approx I^{0.5–0.6}$) in the intensity range 30 W/cm^2 $< I_0 <$ 5 000 W/cm^2. Above 5 000 W/cm^2,

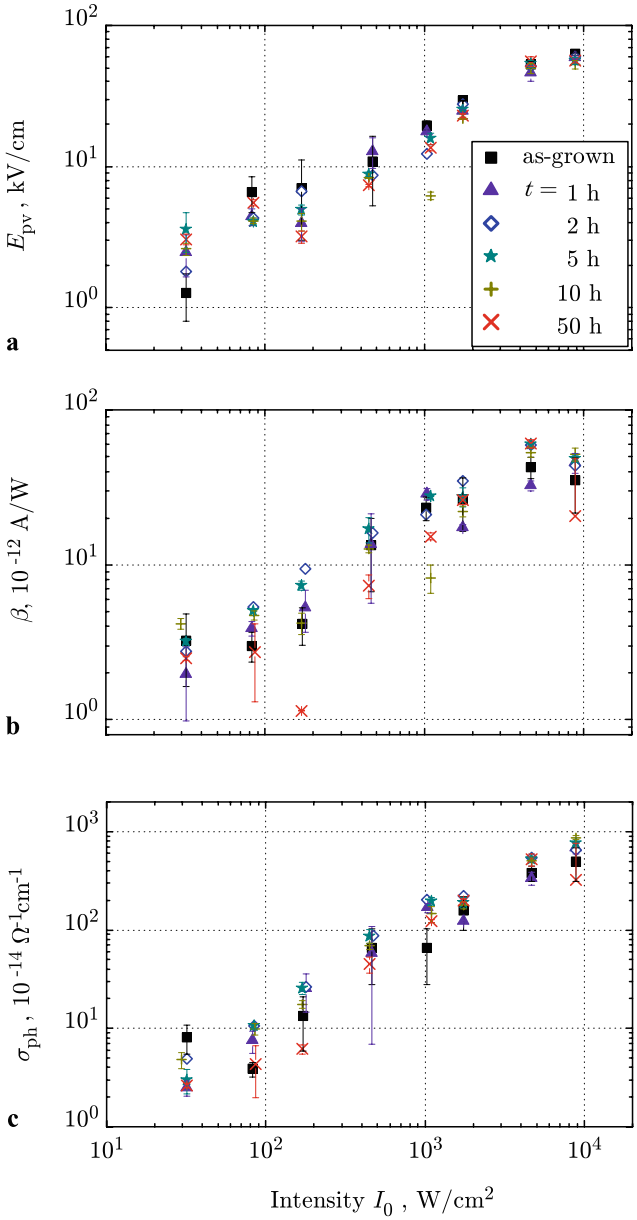

Fig. 3 Intensity dependences of (**a**) the steady-state space-charge field E_{pv}, (**b**) the photovoltaic coefficient β, and (**c**) the photoconductivity σ_{ph} after different oxidization times t of up to 50 h

E_{pv} seems to saturate at values of about 70 kV/cm, which is roughly (1.5–2) orders of magnitude larger than the values of E_{pv} determined for the low-intensity range.

The photovoltaic coefficient $\beta(I)$ shows also a sublinear growth (approximately as $I^{0.5-0.6}$) by more than one order of magnitude in the intensity range 30–5 000 W/cm^2, see Fig. 3b.

The photoconductivity σ_{ph} grows almost linearly in the investigated intensity range. Only for the lowest and highest intensities used (<100 W/cm^2 and >5 000 W/cm^2) small deviations from this behavior towards a sublinear growth appear. In total, σ_{ph} varies by more than two orders of magnitude, from 4×10^{-14} Ω^{-1}cm^{-1} to 7×10^{-12} Ω^{-1}cm^{-1}.

For all three quantities under consideration, E_{pv}, β, and σ_{ph}, the impact of the oxidization treatment is weak. There is a trend that the values are slightly diminished for longer oxidization times. It should be noted that the values of E_{pv}, β, and σ_{ph} for one crystal at a fixed intensity can spread over almost an order of magnitude, as is indicated by the error bars in Fig. 3a–c. This variation of the photoelectric properties over the sample volume slightly decreases with longer oxidization.

A second series of experiments is conducted using the wedge crystal and the 100-µm-thick crystal, both in the as-grown state. With these additional measurements, any possible dependence of the results shown in Fig. 3 on the sample thickness d can be revealed. This time, the radius of the recording beam is $w_{532} = 80$ µm. The results of these measurements are shown in Fig. 4, for comparison together with the results for the 1-mm-thick as-grown crystal, which was investigated with a recording beam radius of $w_{532} = 30$ µm (black squares in Figs. 3 and 4).

Figure 4 shows that there is no thickness dependence for the steady-state values of the field $E_{pv}(I)$ within the measurement accuracy. There is good agreement between the data obtained with the 1-mm samples, the wedge sample with the different thicknesses, and the 100-µm sample. The maximum value of E_{pv} is now measured to be ≈100 kV/cm at an intensity of 30 000 W/cm^2.

The situation for the photovoltaic coefficient β is different, as can be seen in Fig. 4b. The total variation of β over the whole intensity range (30–30 000) W/cm^2, which is proportional to $I^{0.3-0.4}$, is considerably smaller for the data points obtained with the wedge crystal and the thin crystal. The strongest deviation from the values obtained with the 1-mm-thick samples is found for low intensities $I_0 < 500$ W/cm^2.

Considering the results for the photoconductivity σ_{ph}, which are depicted in Fig. 4c, again slight differences are visible, especially in the low intensity regime $I_0 <$ 200 W/cm^2, where the values obtained with the wedge sample and the thin sample are larger than those for the 1-mm samples. Taking the results for the wedge and the thin sample, the photoconductivity shows an intensity dependence being proportional to $I^{0.7}$.

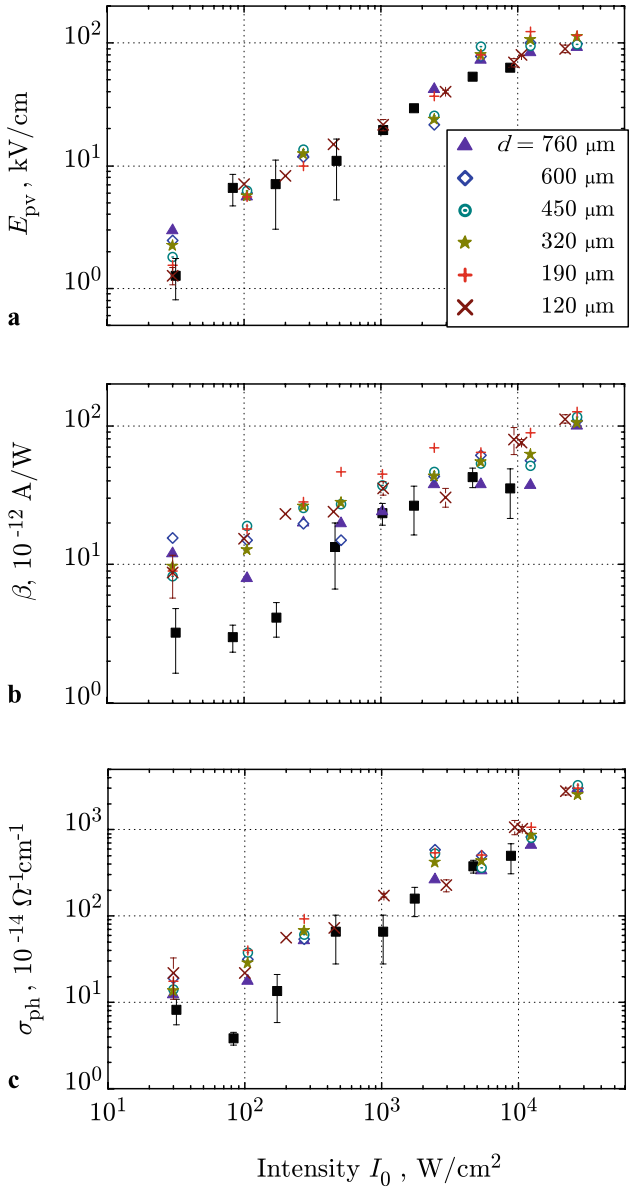

Fig. 4 Intensity dependences for (**a**) the steady-state space-charge field E_{pv}, (**b**) the photovoltaic coefficient β, and (**c**) the photoconductivity σ_{ph} for different crystal thicknesses d. For comparison, the results for the 1-mm-thick as-grown crystal are also shown (*black squares*)

4 Discussion

From the experimental data the following insights can be gained.

Charge transport models: The intensity dependences of the photovoltaic field E_{pv} and of the photovoltaic coeffi-

cient β (Figs. 3 and 4) show that in nominally-undoped crystals one has to consider already at relatively small intensity values a two-center charge transport situation. This confirms earlier results [12, 13].

Oxidization treatment: Conventional oxidization has almost no influence on the charge transport parameters (Fig. 3). We just observe some spatial homogenization of the photoelectric properties. This results probably from thermal excitation of electrons, their random walk, and a—more homogeneous—recombination with deep traps.

Quantitative estimates: Since we do not expect any dependence of the charge transport parameters on the crystal thickness, the spread of the values in Fig. 4 for a certain intensity gives an estimate of the accuracy of the data. Since beam distortion may change the profile of the pump beam in the rear crystal part, the data obtained for the thinnest sample is probably the most reliable.

Because evaluation of the data within the one-center model requires less assumptions and because this model is known to be valid for the smallest intensities used in this study—about 30 W/cm^2—, the one-center model is appropriate to draw some conclusions.

Typical values of $\beta^*_{\mathrm{Fe}} = \beta / c_{\mathrm{Fe}^{2+}}$ for moderately iron-doped crystals are (6–8) $\times$ 10^{-33} Am^3/W [24]. Assuming a linear dependence between β and the Fe^{2+} concentration $c_{\mathrm{Fe}^{2+}}$, we deduce from $\beta_{30\,\mathrm{W/cm^2}} \approx 10^{-11}$ A/W a value of $c_{\mathrm{Fe}^{2+}} \approx 10^{15}$ cm^{-3} for our undoped samples. For an assumed total iron concentration of about 1 ppm $\equiv 2 \times 10^{16}$ cm^{-3}, this corresponds to an oxidization state of $\approx$0.06, which is very reasonable for such doping levels. With this value for the Fe^{2+} concentration, we are also able to exclude space-charge limitations for our experimental conditions. The corresponding field $E_{\mathrm{q}} \approx e w_{532} c_{\mathrm{Fe}^{2+}} / \varepsilon \varepsilon_0 =$ 500 kV/cm with $w_{532} = 80$ µm is much larger than the largest values measured for the photovoltaic field E_{pv}.

Now let us take a look at the photoconductivity. For an intensity of 30 W/cm^2, we measure $\sigma_{\mathrm{ph}} \approx 1.5 \times 10^{-13}\ \Omega^{-1}\mathrm{cm}^{-1}$, which gives $\sigma_{\mathrm{ph}}/I \approx 5 \times 10^{-15}$ cm/ΩW. Using the Fe^{2+} concentration given above, we can estimate for our nominally-undoped crystals a value of the lifetime-mobility product $\mu_{\mathrm{e}}\tau_{\mathrm{e}} \approx 2.5 \times 10^{-12}$ cm^2/V. For moderately doped crystals with an oxidization state $\approx$0.05, we have $\mu_{\mathrm{e}}\tau_{\mathrm{e}} \approx 1 \times 10^{-13}$ cm^2/V, which is considerably smaller than our value for the $\mu_{\mathrm{e}}\tau_{\mathrm{e}}$ product. This agrees with our expectations: due to the smaller concentration of deep traps c_{Fe}, the recombination time τ_{e} should be larger in nominally-undoped crystals. Thus, the product $\mu_{\mathrm{e}}\tau_{\mathrm{e}}$ should also be larger, as is indeed the case.

5 Summary

We provide reliable data on the charge transport properties of congruent, nominally-undoped as-grown and oxidized $LiNbO_3$ crystals. The data were obtained from time-resolved birefringence measurements.

The dependences of the saturation space-charge field E_{pv} and the photovoltaic coefficient β over a wide intensity range of (30–30 000) W/cm^2 can be explained using the two-center charge transport model, and they are in accordance with those of earlier publications.

The findings are of relevance for achieving a better understanding of optical damage in nominally-undoped, congruent $LiNbO_3$ crystals. They will help to improve methods for the suppression of optical damage in such crystals, e.g., optical cleaning [20].

Acknowledgement Financial support from the DFG research unit 557 and the Deutsche Telekom AG is gratefully acknowledged.

References

1. Y.S. Kuzminov, *Lithium Niobate Crystals* (Cambridge International Science, Cambridge, 1999)
2. L.E. Myers, R.C. Eckardt, M.M. Fejer, R.L. Byer, W.R. Bosenberg, J.W. Pierce, J. Opt. Soc. Am. B **12**, 2102 (1995)
3. N.G.R. Broderick, G.W. Ross, H.L. Offerhaus, D.J. Richardson, D.C. Hanna, Phys. Rev. Lett. **84**, 4345 (2000)
4. A. Ashkin, G.D. Boyd, J.M. Dziedzic, R.G. Smith, A.A. Ballman, J.J. Levinstein, K. Nassau, Appl. Phys. Lett. **9**, 72 (1966)
5. P. Günter, J.-P. Huignard, *Photorefractive Materials and Their Applications I, II* (Springer, New York, 2006, 2007)
6. A.M. Glass, D. von der Linde, T.J. Negran, Appl. Phys. Lett. **25**, 233 (1974)
7. L. Solymar, D. Webb, A. Grunnet-Jepsen, *The Physics and Applications of Photorefractive Materials* (Clarendon, Oxford, 1996)
8. K. Buse, Appl. Phys. B **64**, 391 (1997)
9. K. Buse, Appl. Phys. B **64**, 273 (1997)
10. V. Fridkin, B. Sturman, *The Photovoltaic and Photorefractive Effects in Noncentrosymmetric Materials* (Gordon and Breach, New York, 1992)
11. B. Sturman, J. Opt. Soc. Am. B **8**, 1333 (1991)
12. O. Althoff, A. Erdmann, L. Wiskott, P. Hertel, Phys. Stat. Sol. A **128**, K41 (1991)
13. F. Jermann, J. Otten, J. Opt. Soc. Am. B **10**, 2085 (1993)
14. F. Jermann, M. Simon, E. Krätzig, J. Opt. Soc. Am. B **12**, 2066 (1995)
15. F.S. Chen, J. Appl. Phys. **40**, 3389 (1969)
16. A. Yariv, P. Yeh, *Optical Waves in Crystals* (Wiley, New York, 2003)
17. M. Kösters, B. Sturman, D. Haertle, K. Buse, Opt. Lett. **34**, 1036 (2009)
18. W. Phillips, D.L. Staebler, J. Electron. Mater. **3**, 601 (1974)
19. D. Sugak, Y. Zhydachevskii, Y. Sugak, O. Buryy, S. Ubizskii, I. Solskii, M. Schrader, K.D. Becker, J. Phys.: Condens. Matter **19**, 086211 (2007)
20. M. Kösters, B. Sturman, P. Werheit, D. Haertle, K. Buse, Nat. Phot., accepted for publication (2009)
21. G.J. Edwards, M. Lawrence, Opt. Quantum Electron. **16**, 373 (1984)
22. M. Jazbinšek, M. Zgonik, Appl. Phys. B **74**, 407 (2002)
23. N.V. Kukhtarev, Sov. Tech. Phys. Lett. **2**, 438 (1976)
24. K. Peithmann, A. Wiebrock, K. Buse, Appl. Phys. B **68**, 777 (1999)